Development and Evaluation of a Digital Radiographic System Based on CMOS Image Sensor

Ho Kyung Kim, Gyuseong Cho, *Member, IEEE*, Seung Wook Lee, Young Hoon Shin, and Hyo Sung Cho

***Abstract*—A cost-effective digital radiographic system with a large field-of-view (FOV) of $17'' \times 17''$ has been developed. The cascaded imaging system mainly consists of three parts: 1) a phosphor screen to convert incident X-rays into visible photons; 2) a matrix of 8×8 array of lens assembly to efficiently collect visible photons emitted by the phosphor screen; and 3) 8×8 complementary metal-oxide-semiconductor (CMOS) image sensors, aligned to the corresponding lens assembly. Although low in cost due to economical CMOS image sensors, the overall performance features are comparable with other commercial digital radiographic systems. From the analysis of signal and noise propagation, the system is *not* an "X-ray quantum-limited" system, rather the system has secondary quantum sink at the light collecting stage. The system resolution is about 2 line pairs per millimeter from both of measured from X-ray images of a line-pair test pattern and the calculation of the modulation-transfer function. Detailed experimental and theoretical analysis of performance will be discussed.**

***Index Terms*—Complementary metal-oxide-semiconductor (CMOS), digital radiography (DR), parallel-hardware architecture, X-ray imaging.**

I. Introduction

FOR THE PAST century, a combination of intensifying screen and film has been the primary diagnostic tool in conventional radiology, and it is still being used due to its inherent good spatial resolution and low cost. However, in recent years, the digitization of medical images, especially in radiology, has been much demanded and is facing a rapid advance in computer-based imaging technologies and picture archival and communications systems (PACS). As alternatives to the screen-film system, various digital imaging systems are being developed; amorphous silicon- [1] and amorphous selenium-based flat panel devices [2]. Antonuk *et al.* [3] summarized active-matrix flat-panel imager development, and the state-of-the-art is the flat-panel imager having the pixel size of $\sim 100\ \mu$m and the total active area of almost 40×40 cm^2, which was made by the tiling of two or four panels.

However, there are still several crucial problems for commercialization such as the low yield of panels in mass production lines and complexity of driving circuitries, so that the cost is very high. As similar approach to our work, Slump *et al.* [4] introduced a matrix of 2×2 charge-coupled device (CCD) sensors optically coupled with phosphor screen for real-time diagnostic imaging. Advantages of this method are the well-developed technologies and commercially availabilities of scintillating phosphor, lens and CCD.

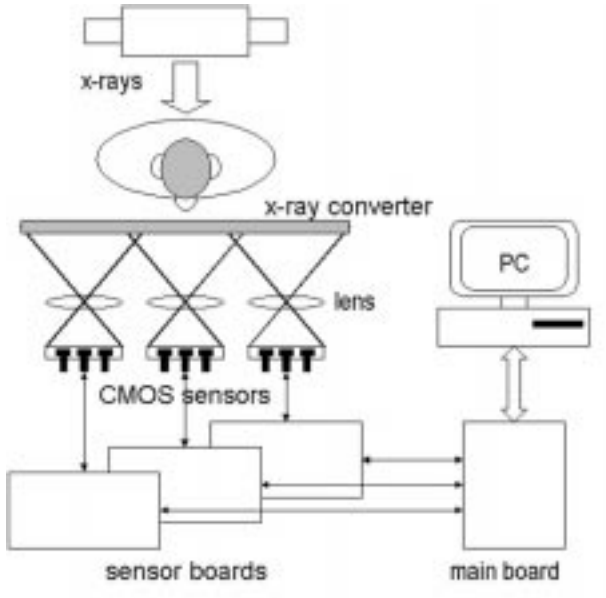

Fig. 1. A schematic illustration of the developmental CMOS-based X-ray imaging system for medical application. Avoiding confusion, only three of the CMOS sensors are showed in this figure.

In this study, we present a cost-effective digital radiographic system based on the complementary metal-oxide-semiconductor (CMOS) image sensor. Due to the modern microelectronic technologies for memory chips and application-specific integrated circuits (ASICs), CMOS sensors have recently achieved significant advantages over CCDs; lower cost (higher yield), lower power consumption and most importantly, higher system integration such as on-chip analog-to-digital conversion circuitries [5]. The main difference between CMOS and CCD pixel structures is the use of amplifying transistors for each pixel in the CMOS structure. In following sections, we describe each component of our detector system in detail, including operation principles. With experimental measurements and first acquired images, the overall performances will be also presented in this manuscript.

Manuscript received October 12, 2000; revised March 29, 2001.

H. K. Kim, G. Cho and S. W. Lee are with the Department of Nuclear Engineering, Korea Advanced Institute of Science and Technology, Taejon 305-701, Korea (e-mail: hokyung@kaist.ac.kr).

Y. H. Shin is with the R&D center, Star V-Ray, TBI, Korea Advanced Institute of Science and Technology, Taejon 305-701, Korea.

H. S. Cho is with the Department of Medical Engineering, Yonsei, University, Wonju 220-710, Korea.

Publisher Item Identifier S 0018-9499(01)05089-4.

II. System Description

A schematic illustration of the developed detector system is shown in Fig. 1. The detector system consists of several components: an X-ray converter screen, lens assembly, CMOS sensors, and readout electronics. The visible photons, resulting from irradiation of a phosphor screen, are collected by the lens assembly. The light is then focused by lens onto the CMOS sensor. An analog-to-digital converter (ADC) is embedded in CMOS sensor, and the digital output is transferred to frame-buffers which are built on a sensor board. CMOS and sensor board are controlled by the main data acquisition board which has a micro-processor. Finally, the image data are transferred to the computer through PCI interface and displayed. For the application to the chest radiography, total 8×8 of lens-CMOS sensor modules are constructed to cover $17'' \times 17''$ active area.In order to support this parallel-hardware-architecture, some software techniques are implemented.

As an X-ray converter, a commercially available phosphor screen (Lanex regular, Eastman Kodak), which gives about 3.6 mm^{-1} at 10% of modulation-transfer function (MTF), was employed. Since our phosphor screen is based on a terbium (Tb) doped Gd_2O_2S, it gives an emission spectrum with the peak at 545 nm.

For the effective transfer of image information from the phosphor screen to CMOS sensors, the lens was carefully designed by using a simulation code, including the effect of stray or ghost light. In our design, light collected through the lens should be focused on a 6 μm-radius spot, where it is noted that the pixel size of our CMOS sensors is 9 μm The developed lens assembly was evaluated by the measurementof MTF. Fig. 2 shows the measurement result, which was conducted in Korea Research Institute of Standards and Science (KRISS), and gives 83 mm^{-1} at 10% of MTF.

The CMOS image sensor used in this study is an active pixel sensor (APS) with 9 μm-pixel pitch (HDCS-2000, Hewlett Packard). Total 3840×3840 pixels were employed so that the system gives 4.2 mm^{-1} resolution on the X-ray converter. However, accounting for the Bayer pattern (i.e., color sensor) of sensor and overlapped regions, which are intersections among the fields of view of each sensor (see Fig. 1) required to register the loss-less image, the achievable maximum theoretical resolution is 2.25 mm^{-1}. Since the sensoris a color sensor, it has some disadvantages for our application, such as the relatively lower quantum efficiency (21% at 545 nm wavelength) and the small fill-factor (42%).

Driving and readout electronics have been built on four sensor-boards and a main data acquisition board is used. Each sensor board is controlled by the main board and acquires images from 16 (or 4×4 sensors with a corresponding frame buffer. The acquired image data is then transferred to a host computer through RS485 with the speed of 2.5 Mb/s. Considering image reconstruction and correction (will be discussed just below), the refresh time to obtain next image is about 20 s.

The procedure of implemented software techniques to support the parallel-hardware-architecture (or mosaic structure) is summarized as follows.

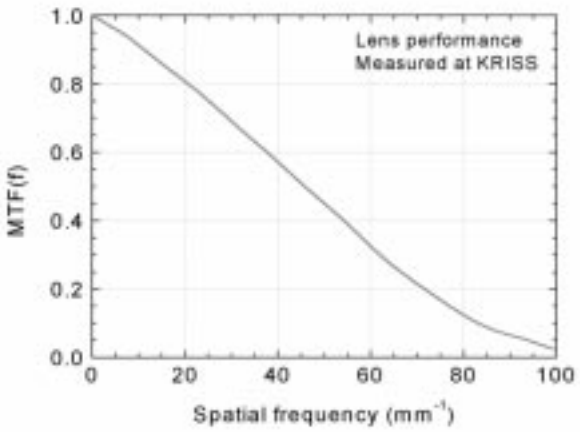

Fig. 2. MTF of the designed lens system, which was measured at Korea Research Institute of Standards and Science (KRISS). It gives more than 80 mm^{-1} at 10%.

(a) Median filtering: In order to correct noisy pixels, typically due to large dark current in fabrication or due to scattered X-ray photon directly absorbed in the pixel during irradiation, eight pixels surrounding the given pixel was considered.
(b) Bayer pattern correction: It is an inevitable process due to the employed VGA color sensor. Regarding the emitted green lights from the phosphor screen, each of red and blue pixels was re-scaled from the surrounding four green pixels.
(c) Brightness correction: For nonlinear sensitivities of 64 sensors, each was calibrated.
(d) Stitching (geometric correction): It is a distortion correction of optical aberrations due to lens and stitches to form a mosaic of 8×8 images based upon the use of a calibration pattern containing fiducial markers.

III. Performance Analysis

A. Lens Coupling Efficiency

Since, generally, the utilization of CCD or CMOS sensor coupled with an X-ray conversion phosphor demagnifies the active FOV into the limited sensor area, the collection efficiency is very small (typically, 0.01%). Therefore, the real-time operation requires high X-ray flux or an intensified sensor. The lens coupling efficiency can be given by [6]

$$\eta_L = \frac{\tau m^2}{m^2 + 4F^2(1+m)^2} \tag{1}$$

where

τ transmission efficiency through the glass of lens;
m magnification factor between the real and the virtual image;
F f-number, focal length divided by aperture of the lens.

Equation (1) is based upon the Lambertian approximation. Since the phosphor screen is usually modeled as a Lambertian source, the use of (1) is reasonable to this study. The calculated efficiency on our system is about 0.04%. For the given three cases

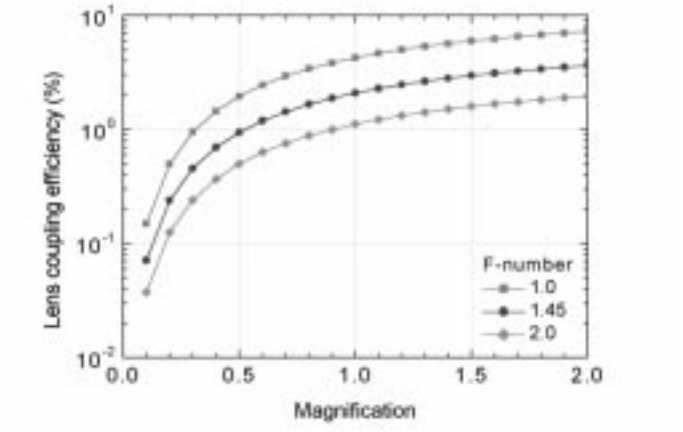

Fig. 3. Lens coupling efficiency with respect to magnification for 3 cases of f-number. It is noted that the efficiency is limited to just a few percents.

of f-number, Fig. 3 shows the lens collection efficiencies as a function of the magnification factor.

B. Signal and Noise Characteristics

The signal and noise transfer characteristics of a cascaded imaging system are generally governed by the number of image quanta propagating through each stage. A quantum accounting diagram (QAD) [7], often used by system designer, is a plot of the effective number of quanta for given spatial frequency as a function of stage number. Using this graph, designers can select specific factors, such as X-ray detection efficiency, amplification factors or coupling efficiencies to prevent or remove secondary quantum sinks and optimize the design of an imaging system. Based on the typical parameter values for our system as shown Table I [8], we examined the QAD at zero spatial-frequency for two different detectors, mainly distinguished in terms of the quantum efficiency and fill-factor, defined as the fraction of the total detector area which is sensitive to the input signal. It is noted that the detector-I (HDCS-2000, VGA-formatted, HP) is currently implemented into our system and the detector-II (IBIS4C, monochromatic, Fillfactory) is considering for next version. The efficiency and gain of the screen $(Gd_2O_2S{:}Tb)$ for mono-energetic incident X-rays of 50 keV energy were obtained from reference [8]. From the Fig. 4, there are two quantum sinks in our system: one at X-ray absorption by the phosphor layer and the other at the light collecting stage as we expected. Since information-carrying quanta are lost irrecoverably in the quantum sink, it limits the signal-to-noise ratio (SNR) of the whole system. Therefore, we need to increase the number of quanta at the light collecting stage by improving the lens system. In order to avoid further loss of information-carrying quanta after the light collecting stage, the choice or design of photo-detector with high quantum efficiency and large fill-factor is important.

Fig. 5 plots the noise versus the exposure of our detector system in logarithmic scales. The slope of fitted curve on the experimentally determined data points is 0.44. In a system for which X-ray quantum noise is the dominant noise source, the slope of such a plot is approximately 0.5 as indicated by the dotted line in Fig. 5. A slope less than 0.5 indicates the presence of significant contributions to the noise components from sources other than X-ray noise. From the result, oursystem is not an "X-ray quantum-limited" system, and there exists another source of noise contributing the total system performance, which is probably a readout noise during exposure.

TABLE I
GAIN OR EFFICIENCY OF EACH COMPONENT

Stage	Description	Value
1	Incident x-ray quanta on phosphor screen	1
2	Detection efficiency of phosphor screen	0.5
3	Average phosphor screen gain in emitted optical photons per absorbed x-ray quantum	1,500
4	Collection efficiency of optical photons by lens	0.0004
5	Fraction of photo-sensitive area of detector	0.42 for detector-I 0.6 for detector-II
6	Quantum efficiency of detector in signal electrons created per collected optical photon	0.21 for detector-I 0.5 for detector-II

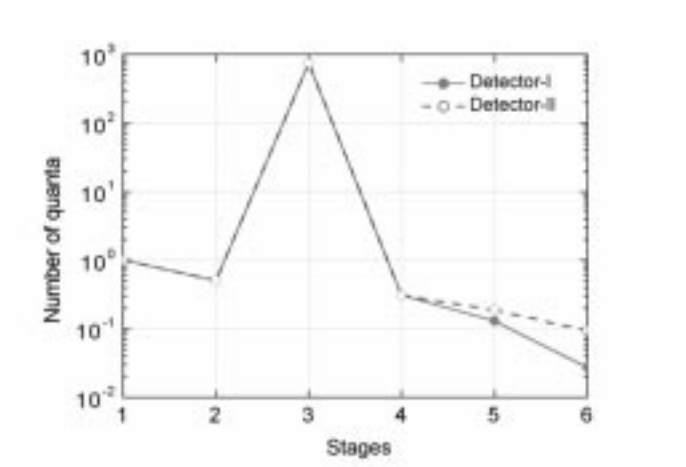

Fig. 4. Quantum accounting diagram as a function of stage.

C. System Modulation Transfer Function

The spatial resolution of an imaging system is usually characterized by the MTF, which defined as the ratio of the output modulation to the input modulation for a sinusoidal input signal as a function of spatial frequency. We obtained the MTF for our system from the measurement of edge-spread function (ESF). The line-spread function (LSF) can be obtained by the derivative of ESF, and then the MTF by the Fourier transformation of LSF. Fig. 6 shows the system MTF based on the measured ESF. Our developmental system gives about 2 mm^{-1} at 10% of the calculated MTF. It is noted that the maximum theoretical resolution of the CMOS sensor is 2.25 mm^{-1}, as discussed in the above.

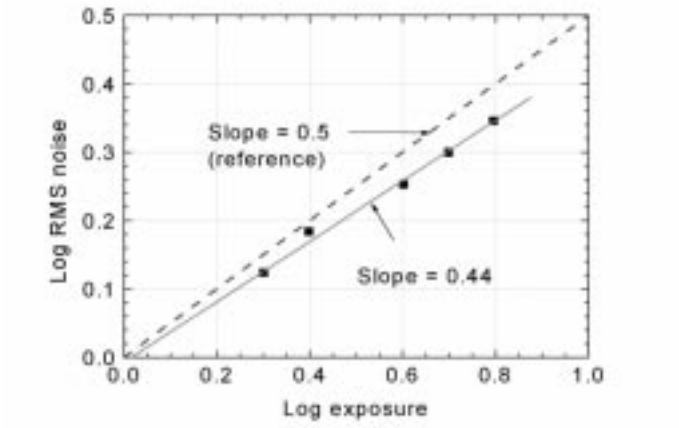

Fig. 5. System noise as a function of exposure. The system noise increases linearly with a slope of 0.44, which means the presence of another noise source other than X-ray noise. The dotted line is a reference showing an X-ray quantum-limited system.

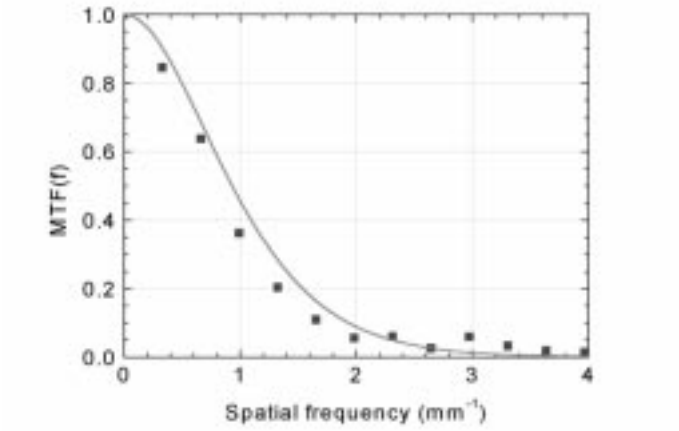

Fig. 6. System MTF of our system, which was calculated from the measurement of ESF.

D. Acquired Images

Fig. 7 shows examples of X-ray images: (a) line-pair testpattern, (b) a real human hand acquired at 80 kV_p, and (c) chest at 95 kV_p. Taking an X-ray image of the line-pair test pattern showed that our developmental system could resolve about 2 line-pairs per millimeter, which is supported by the calculated system MTF discussed in the above.

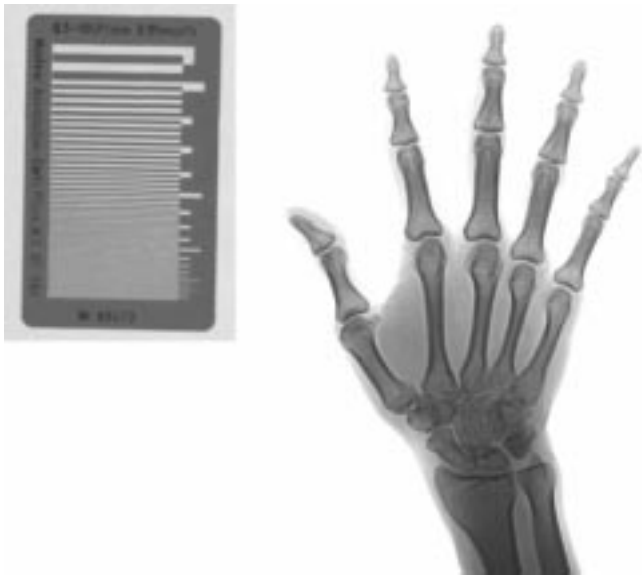

(a) (b)

(c)

Fig. 7. Examples of X-ray images obtained by the developmental detector system: (a) line-pair test pattern, (b) human hand (80 kV_p), and (c) chest (95 kV_p.

IV. Summary and Discussion

We have developed an X-ray imaging system with a large FOV using the CMOS image sensors. For the FOV of $17'' \times 17''$, a mosaic architecture was employed using an array of 8×8 CMOS sensors. We believe that this is the first CMOS-based X-ray imaging system applied to medical chest radiography. In combination of an X-ray conversion method, however, the use of optical coupling by lens mainly degrades the overall system performances due to the low light collection efficiency (0.04% in this study), resulting to the secondary quantum sink. The use of VGA-formatted CMOS sensor is another disturbance to reduce the resolution performance by factor of approximately 2. From the measurement of spatial resolution by MTF and line-pair test pattern image, our system is about 2 line-pairs per mm. If we implement a CMOS sensor with monochromatic format (black and white) and large fill-factor, the system performance may be upgraded more than a factor of 2 in spatial resolution and 3.4 in sensitivity. Since the CMOS technology is still growing and the performance is now almost the same as CCD, the CMOS sensor has great potential in the X-ray imaging application.

Our imaging system based on CMOS imager is under investigation for other X-ray imaging applications: 3-dimensional micro-tomography for osteoporosis and laminographic system for the inspection of chip soldering onto printed circuit boards (PCB's). Both of applications need a fine-focus X-ray

tube with the virtual point source, and the magnification in images. Recently, we have installed tomographic system for the cone-beam X-ray source: fine-focus X-ray tube, rotational stage, and CMOS-based X-ray imaging detector [9]. Further studies for radiographic and tomographic system are in progress with CMOS sensors having better performance.

REFERENCES

[1] R. L. Weisfield, M. Hartney, R. Schneider, K. Aflatooni, and R. Lujan, "High performance amorphous silicon image sensor for X-ray diagnostic medical imaging applications," *Proc SPIE*, vol. 3659, pp. 307–317, 1999.

[2] D. L. Lee, L. K. Cheung, and L. S. Jeromin, "A new digital detector for projection radiography," *Proc SPIE*, vol. 2432, pp. 237–249, 1995.

[3] L. E. Antonuk, Y. El-Mohri, A. Hall, K-W. Jee, M. Maolinbay, S.C. Nassif, X. Rong, J. H. Siewerdsen, Q. Zhao, and R. L. Weisfield, "A large-area, 97 μm pitch, indirect-detection, active matrix, flat-panel imager (AMFPI)," *Proc SPIE*, vol. 3336, pp. 2–13, 1998.

[4] C. H. Slump, G. J. Laanstra, H. Kuipers, M. A. Boer, A. G. J. Nijmeijer, M. J. Bentum, R. Kemner, H. J. Meulenbrugge, and R. M. Snoeren, "A novel X-ray detector with multiple screen-CCD sensors for real-time diagnostic imaging," *Proc SPIE*, vol. 2780, pp. 450–461, 1996.

[5] S. T. Smith, D. R. Bednarek, D. C. Wobschall, M. Jeong, H. Kim, and S. Rudin, "Evaluation of a CMOS image detector for low cost and power medical X-ray imaging applications," *Proc SPIE*, vol. 3659, pp. 952–961, 1999.

[6] T. Yu and J. M. Boone, "Lens coupling efficiency: Derivation and application under differing geometrical assumptions," *Med Phys*, vol. 24, pp. 565–570, 1997.

[7] I. A. Cunningham, M. S. Westmore, and A. Fenster, "A spatial-frequency dependent quantum accounting diagram and detective quantum efficiency model of signal and noise propagation in cascaded imaging systems," *Med Phys*, vol. 21, pp. 417–427, 1994.

[8] S. Hejazi and D. P Trauernicht, "System consideration in CCD-based X-ray imaging for digital chest radiography and digital mammography," *Med Phys*, vol. 24, pp. 287–297, 1997.

[9] S. W. Lee, H. K. Kim, G. Cho, Y. H. Shin, and Y. Y. Won, "A 3D microtomographic system with CMOS image sensor," in *IEEE Medical Imaging Conference*, Oct. 15–30, 2000.